Water & surface contamination monitoring using deep UV laser induced native fluorescence and Raman spectroscopy

Article *in* Proceedings of SPIE - The International Society for Optical Engineering · October 2006

DOI: 10.1117/12.686487

Water & Surface Contamination Monitoring Using Deep UV Laser Induced Native Fluorescence and Raman Spectroscopy

William F. Hug[*a], Rohit Bhartia[b], Alexandre Tsapin[b],
Arthur Lane[b], Pamela Conrad[b], Kripa Sijapati[a], Ray D. Reid[a],
[a]Photon Systems, Inc., 1512 Industrial Park St., Covina, CA 91722
[b]Jet Propulsion Laboratory, Caltech, 4800 Oak Grove Dr., Pasadena, CA 91109

Abstract

Reagentless water and surface sensors employing laser induced native fluorescence (LINF) and resonance Raman spectroscopy (RRS) in the deep UV are making significant progress in detecting chemical and biological targets and differentiating them against a wide range of background materials. Methods for optimizing sensor performance for specific target and backgrounds materials will be discussed in relationship to closed industrial environments and open natural environments. Limits of detection and chemical specificity will be discussed for high and low spectral resolution systems for a wide range of compounds and composite particles such as spores and cells. Detection and identification of single spores at working distance of several meters is illustrated.

A range of sensors will be described along with their physical and performance specifications including sample, sipper and immersion sensors for water and fixed point and scanner systems for surfaces. In addition, the use of UV LINF and RRS for detection in capillary electrophoresis and liquid chromatography will be described with limits of detection in the range of a few nmol L^{-1}.

Keywords: native fluorescence, resonance Raman, biological and chemical contamination detection

1. INTRODUCTION

Testing methods for microbial and chemical contamination traditionally require considerable consumables and human time. The most common method requires taking a sample using a swab for surface contamination or rinsing or otherwise extracting the contaminant from a filter or other concentrator for air or water contamination. For biological contamination, the sample is then cultured until enough microorganisms exist to be visible as a colony on a petri dish. Traditionally, for biology, this method takes days to weeks and requires growth media, petri dishes and other consumables. The method is flawed not only because of the time and consumables needed, but also because it provides incomplete information. It is known that less than 1% of all viable microbes are culturable. 99% of all bacteria and archea revealed by broad-range DNA sequence "mining" on Earth cannot be cultured in the laboratory[1]. The rapidly evolving instruments for genetic sequencing are the ultimate method of identifying microbes but require wet chemistry with significant sample preparation. Portable instruments based on high-density DNA hybridization microarray technologies are also improving rapidly. These technologies require significant consumables and human preparation and analysis time and require significant sample sizes.

Photon Systems and other organizations are proposing a variety of optical techniques for in situ, non-contact, detection and identification of biological as well as chemical warfare agents and other municipal, industrial, or commercial contaminants. Optical, and especially ultraviolet (UV) optical, techniques are being proposed because they typically require no sample preparation or handling and are generally easy to use and rapid compared to wet-chemistry techniques presently being employed. Ultraviolet methods are especially important because they eliminate the need for derivatization of a sample, which requires sample handling and adds considerable complexity to the detection and identification process. Derivatization is also an imperfect process that interferes with the basic chemistry being elucidated. The ability to optically discriminate microbes or other contaminants from complex backgrounds and classify them, with low false alarm rates, depends of the ability of a proposed technique to accurately measure and relate spectroscopic chemical signatures to essential features of the microbes or chemicals under investigation. False alarm rate depends strongly on the excitation and observation wavelengths employed and the algorithms used to discriminate good from bad. Our focus is on UVLINF and UVRRS because we believe these techniques are the only viable high-sensitivity microbial and chemical measurement techniques that could be deployed in a low power, miniature, robust,

and inexpensive package. As will be shown below, integration of UVLINF and UVRRS is an ideal marriage since native fluorescence offers very high sensitivity with some level of specificity and pre-resonance and resonance Raman offers a much higher level of specificity at reduced sensitivity and both spectral measurements can be performed simultaneously in well segregated spectral regions.

Recently a major breakthrough in the performance of our deep UV 224.3 nm HeAg and 248.6 nm NeCu has enabled a wider range of uses of these lasers for microbial and chemical contamination, including proximity stand-off detection using native fluorescence and Raman. These lasers have construction similar to miniature klystrons or traveling wave tubes and operate at ambient temperature without warm-up, pre-heating or temperature regulation. The lasers have been tested from –100C to +60C and come to full power within about 10 μs of triggering, independent of ambient conditions. These lasers were recently tested to launch and landing shock and vibration conditions for a space mission to the planet Mars. The range of UV emission wavelengths offered by these lasers is important to enabling native fluorescence and fluorescence-free resonance Raman spectroscopy of a wide range of biological and organic materials. The 224 nm HeAg and 248nm NeCu lasers emit between 10 μJ and 60 μJ of energy and require only 0.2J to 0.6J of electrical input energy. This corresponds to between 10^{12} and 10^{14} photons per pulse, an adequate amount to obtain native fluorescence and Raman spectra. The pulses are soft compared to harmonic generated outputs from diode pumped solids state (DPSS) lasers with output between 20 mW and 1.8W when compared to many kW or MW from DPSS lasers. Typically, complete spectra are obtained in a single laser pulse so that at sample rates of a few Hz the average power consumption of the laser is less than few watts. And no heating or temperature regulation is required. This is significant since other lasers emitting in this wavelength range typically consume over 10kW to 15kW. The linewidth and frequency stability is less than 0.07 cm^{-1} or 0.4 pm and is independent of ambient conditions. Because of the fast turn-on time these lasers are ideal for triggered response to particles on-the-fly. Additional advantages of these new lasers are their small size, weight, and very low cost.

2. INTEGRATION OF UV RAMAN AND NATIVE FLUORESCENCE

2.1 Combining Raman and native fluorescence in the UV

Rayleigh, Raman, luminescence, fluorescence and phosphorescence emissions from a sample provide an enormous range of information about the sample chemistry and construction. Most biological and organic materials absorb strongly in the deep UV, corresponding to their first electronic state, and emit fluorescence and phosphorescence at longer wavelengths. Luminescence, fluorescence and phosphorescence spectra are independent of excitation wavelength. Asher[2] showed that the range of emission wavelengths due to these processes is generally limited to wavelengths above about 260nm. Very few materials fluoresce or phosphorese below this wavelength. Raman spectra, on the contrary, are dependent on the excitation wavelength and are measured in molecular vibration energy terms above (Stokes) or below (anti-Stokes) the excitation wavelength. Therefore, as the excitation wavelength is reduced below the lower limit of fluorescence, there is a fluorescence-background-free region above the excitation wavelength in which to observe the normally weak Raman emissions. Figure 1, below, graphically illustrates this.

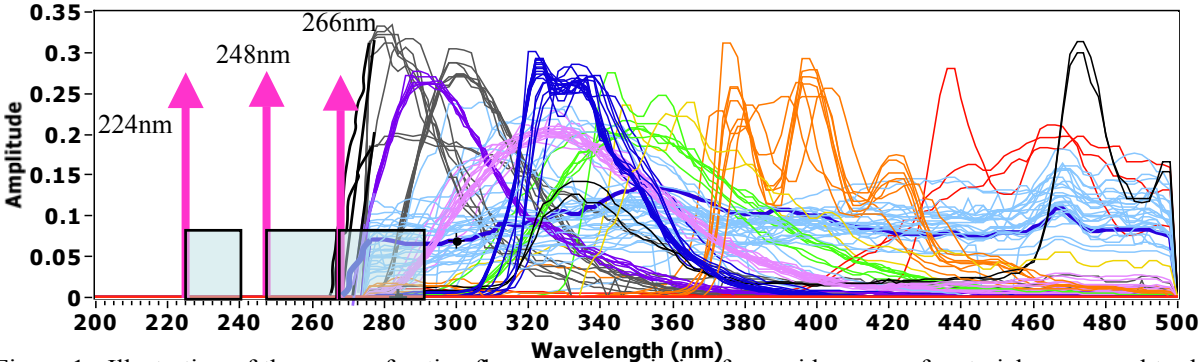

Figure 1. Illustration of the range of native fluorescence emission for a wide range of materials compared to deep UV Raman emission ranges with excitation at 224nm, 248nm, and 266nm lasers

The pale blue band above each of the excitation wavelengths shown in Fig.1 correspond to a 3000 cm^{-1} Raman shift range. Illustrated is the fact that excitation at 224nm provides a fluorescence-background-free range for well over 3000

cm^{-1}. Excitation at 248nm is fluorescence-background-free for all but a few material, and only at the largest Raman shifts. Excitation at 266nm occurs directly in the middle of the native fluorescence of a wide range of biological and organic chemical materials. In addition, the water Raman band for a 266 nm laser occurs in the middle of biological native fluorescence bands, making it difficult to use these lasers for biological identification using native fluorescence. And excitation at longer wavelength further exacerbates the problem of fluorescence interference, just as the Raman signals themselves are diminished by Rayleigh law and other considerations. Raman spectroscopy conducted in the deep UV has five primary advantages over near UV, visible or near-IR Raman spectroscopy summarized as: Rayleigh law, resonance Raman, simplification of spectra, and fluorescence-free, and solar-blind background.

Raman scatter cross section of any material depends as the inverse fourth power on excitation wavelength, called the Rayleigh scattering law. The Raman cross-section of any Raman band is 20X larger at 248nm than at 532nm and 100 times larger than at 785nm. Overlayed on this signal improvement are pre-resonance or resonance effects which can provide additional increase in Raman cross-sections by factors of 5 or 10 up to several million times. Just between excitation at 532 nm and 248 nm pre-resonance effects for water increase the Raman cross-section about 6X for a total Raman cross-section increase due to Rayleigh and pre-resonance of 120X. The Raman cross-section of water, including both Rayleigh and pre-resonance effects, is 570X between 785 nm and 248 nm. This means that a 785 nm laser requires 570X more power to achieve the same Raman signal as a 248 nm laser. The additional signal enhancement is due to pre-resonance of the water molecule, illustrated by the fact that the experimental data most closely follows the Albrecht A-term in which the lowest electronic state dominates the pre-resonance intensity enhancement[3] The Albrecht A-term expression gives the following frequency dependence of the Raman cross sections.

$$\sigma_R = A \times \nu_o(\nu_o - \nu_R)^3[((\nu_e^2 + \nu_o^2)/ (\nu_e^2 - \nu_o^2)^2) + B]^2 \qquad \text{Equation 1}$$

where ν_R = the Raman frequency (cm^{-1}); ν_o = the laser frequency (cm^{-1}); ν_e = the frequency of the transition to the excited state (cm^{-1}), and A and B = constants. The parameters A, B and ν_e are adjusted to fit the curve to the experimental σ_R versus ν_o data.

When the difference between the laser excitation frequency, ν_o, and the frequency of the transition to the excited electronic state, ν_e, goes to zero, the Raman scatter cross-section in Eq. 1 $[(\nu_e^2 + \nu_o^2)/ (\nu_e^2 - \nu_o^2)^2]$ goes to infinity. In practice, the cross section goes to a very large value, in the millions, but not infinity. Resonance Raman is especially important for organic and biological molecules since strong absorption typically occurs in the deep UV and resonance enhancements of millions of times have been reported[4].

One of the factors limiting the enhancement of Raman scattering when excitation is at or near resonance is absorption of the excitation energy as well as self-absorption of the Raman scattered radiation within the scattering molecules. The Raman signal detected by a sensor is proportional to the Raman cross section, σ_R, the molecular density of the scattering material, ρ, and the amount of absorbance of the laser penetration into the absorbing material at the laser wavelength, α_o, as well as the amount of absorbance of the Raman scattered light reabsorbed by the sample, as described below

$$\text{Eq. 2.} \quad \text{Raman signal} \propto \sigma_R \times \rho \int_0^D 10^{-(\alpha_o + \alpha_R)r} dr \qquad \text{Equation 2}$$

where ρ = molecular density, D = sample thickness, α_o = absorbance per unit length at the laser wavelength, and α_R = absorbance at the Raman emission wavelength[5]. When looking for trace levels of contamination where contaminating materials or particles are of the size of 1 μm to 10 μm, this is not expected to be a limiting problem. The third advantage of operating in the deep UV where electronic resonance effects are important is that the Raman spectra are simplified since resonance enhancement occurs only within the Raman bands associated with the electronic transition[6]. Simplification of the Raman band structure enables easier interpretation of results, which often include complex overlapping band structures for organic and biological materials with normal Raman scattering[7,8].

The fourth very important advantage of operating in the deep UV below about 250nm is the absence of background fluorescence in the Raman spectral range. Raman scattering is a far less efficient process than Rayleigh scattering or fluorescence. Typically Raman scattering is 10^4 to 10^8 times less efficient than fluorescence. Therefore if any

fluorescence process occurs within the target molecules or surrounding materials within the exposure volume of the excitation laser beam, it will overwhelm the weak Raman emissions. For excitation in the visible, the fluorescence efficiency of many materials is over 10,000 to 100,000 times greater than Raman scattering efficiency. Even in the deep UV fluorescence is still at least 500 to 1000 times greater than Raman scattering, unless excitation occurs below about 250nm. Asher[2,3,7] showed that organic materials did not fluoresce below a wavelength about 270nm, independent of the excitation wavelength. This was further proven in many subsequent publications such as Nelson (ref. 8), Sparrow[6], Wu[9], and many others. Therefore, when excitation occurs below about 250nm, a fluorescence-free region extends from the excitation wavelength to over 4000 cm^{-1} in which to observe Raman spectra. This is not the case for lasers that provide excitation at longer wavelengths. Even excitation at 266nm from a 4th harmonic Nd-YVO_4 laser, or equivalent, has most of it's Raman spectral range overlapped with fluorescence from a wide range of organic and mineral materials as illustrated in Fig. 1.

The final advantage of operating in the deep UV is elimination of solar background. Solar background is essentially eliminated below about 300 nm. But the addition of the gated detection described later also serves to reduce the effect of any solar background.

It is therefore ideal to combine UV resonance fluorescence and resonance Raman spectroscopy to form an integrated tool for both detection and identification of biological and chemical contaminants since these methods offer a great combination of sensitivity and specificity that do not share overlapping observation wavebands and both modes of detection can be employed simultaneously.

2.2 Sensitivity of UV resonance Raman and native fluorescence

To quantify the sensitivity of UV resonance Raman and native fluorescence using a 248 nm NeCu laser, Fig.2 below shows the number of detectable particles of a contaminant (biological or organic) within the laser beam spot as a function of working distance between the sensor and the target surface. The sensor has a 13 cm excitation and collection aperture and 6 x 10^{13} photons per pulse at 248 nm.

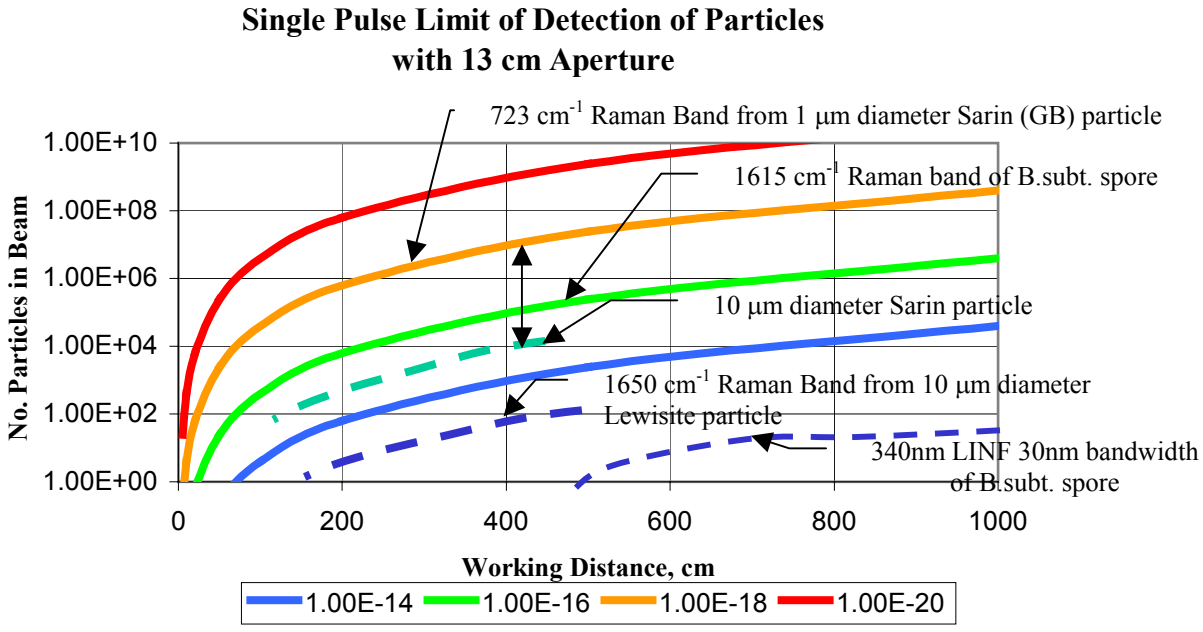

Figure 2. Single pulse limit of detection for biological and organic particles versus working distance

In Fig. 2 curves are shown for LINF detection of B. subtilis spores using a 30 nm wide detection band centered at 340 nm where about 60 spores are detectable during a single laser pulse at a distance of 10 m. Similarly, the 1650 cm^{-1} Raman band of less than 100 particles (10 µm in diameter) of the non-fluorescent chemical agent lewisite, are

detectable with a single laser pulse at a distance of about 4 m. The electrical energy required for this detection is only about 0.5 J.

2.3 Specificity of UV Raman and native fluorescence

We have previously shown that separation of target molecules and particles from background materials can be effectively accomplished with excitation in the deep UV at wavelengths below about 240 nm[10,11]. This is illustrated in Fig. 3 below at an excitation wavelength of 235 nm but separation is nearly as effective at 224 nm. This was determined by using a multivariate technique, Principal Component Analysis (PCA), to compare EEM spectra of 10 groups of targets and background materials. The target groups consisted of 1 ring aromatic amino acids and other compounds (A1 and A2), bacterial spores (B), vegetative bacterial cells (Gram + and Gram -) with cellular components (C), 2 ring aromatics (D), indole-like organics (E) including tryptophan, 3 ring polyaromatic hydrocarbons (PAHs) (F), 4 ring PAHs (G), and >5 Ring PAHS (I). A "background" group (H), consisting pollen, dust, minerals, and household materials (sugar, flour, corn starch, etc), was shown not to interfere with the target groups.

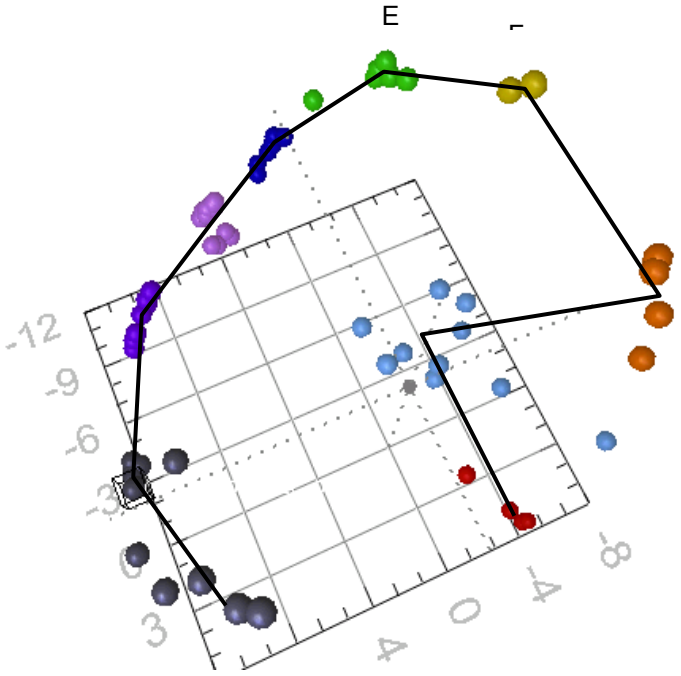

Figure 3. Differentiability of Bacterial spores and vegetative cells from other organic and inorganic background materials with LINF alone.

UV Raman spectroscopy has been demonstrated to be effective in more firmly identifying target materials (Refs. 5, 8, 9, 12, and 13). The specific ability to differentiate against various background materials is not addressed here.

3. TARGETED UV CHEMICAL SENSORS (TUCS)

Targeted ultraviolet chemical sensors (TUCS) are sensors based on combinations of deep UV Raman and native fluorescence spectroscopy. We have built these hand held and portable field sensors in a wide variety of types to fit specific missions, most of which have to date been in extreme environments from Antarctica, to the Arctic, to the deep ocean. In addition to the deep UV lasers we have developed a variety of plug and play components that work with our deep UV lasers to enable the construction of a wide variety of instruments. The lasers and these plug-and-play components are described below.

3.1 Deep UV lasers

The lasers themselves are comprised of a laser tube and laser controller. The all-metal-ceramic construction of these lasers is similar to miniature klystrons or traveling wave tubes (Figs 4 & 5). The laser tubes are all 1.5" in diameter but vary in length from about 5" to 18" depending of the energy or power requirements or working distance of the application. Laser tubes with diameter about 0.75" diameter are in development. The output energy is roughly proportional to length. The tubes weight less than a pound and require about 0.5 J of electrical input to produce up to about 2W of output in the deep UV. Output energy ranges from a few μJ to over 50 μJ. Pulse widths can be digitally controlled from about 10 μs to over 100 μs. Operation of the lasers with their controllers is fully digital with control of pulse width, pulse amplitude and pulse shape. Typical rise time of the laser is about 10 μs so these lasers are compatible with synchronized detection of particles on-the-fly. The lasers operate at ambient temperatures from –100C to +60C without the need for warm-up, pre-heating, or temperature regulation. These lasers can stay dormant for hours or months and come to life upon triggering at full power in about 10 μs and stay on until commanded to turn off. Turn-off time is also about 10 μs. The lasers are very rugged and reliable and have been shock and vibration tested to launch and landing specification of a space mission to Mars. During normal use complete spectra are obtained using only a one or a few pulses of the laser. Lifetime of these lasers is between 10 and 50 million pulses, corresponding to field lifetimes of a few years at spectral sample rates of several Hz. When compared to frequency doubled argon lasers that emit in the same wavelength range, these lasers are 500X smaller and lighter, consume 3000X less power, and are 20X to 50X less expensive. Figure 6 shows a laser tube and controller integrated into a single package although separate packaging is common, depending on the sensor in which they are employed. The research-grade laser controller shown in Fig. 6 is about 2.5" x 9" x 0.75". Much smaller controllers are possible with the smallest being about 2" cube, depending on the sample rate. The average power consumption of this laser is typically less than 5 W, most of which is housekeeping power.

Figure 4. Photo of deep UV laser tube

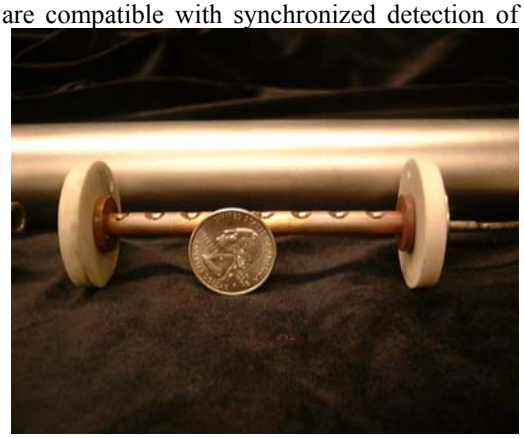

Figure 5. Tube construction similar to traveling wave or klystron tubes

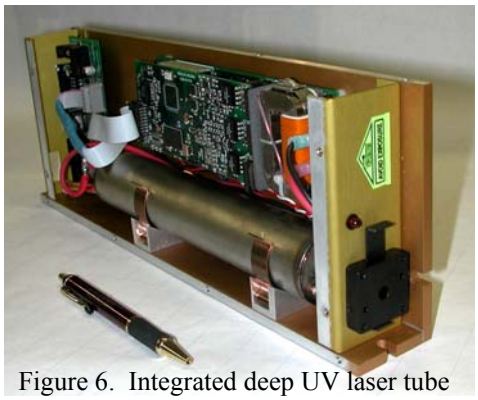

Figure 6. Integrated deep UV laser tube and controller

Interface to the laser is via USB or Ethernet and power is 24 VDC. Each laser and related sensor with all of its stepper motors, shutters, pumps, LEDs, etc. has its own IP address and has been demonstrated to operate and be controllable worldwide over the internet.

3.2 Plug and play sensor components

Built into the laser controller is an RS 488 interface that allows control of a variety of detection systems, stepper motors with encoders, shutters, switches, solenoids, LEDs, pumps, etc. that together are employed in any of a variety of sensors.

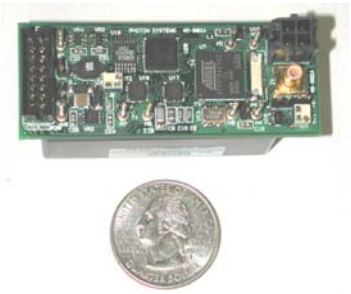

Figure 7. Single-channel digital detector controller

Digital detector controllers (DDCs) come in two varieties: single and multi-channel, shown in Figs. 7 and 8 below. The DDCs allow plug-and-play synchronization of detection with the output of our deep UV lasers. The digital detector controller is designed to interface with commercially available PMTs or photodiodes and include control of the detector as well as provide digital boxcar integration, averaging and 16 bit output digitizing. For specific use with Hamamatsu PMT modules, these controllers allow digital control of detector gain and digitally controllable integration of PMT output current into one of three digitally selectable capacitors (47pf, 470pf, and 4700pf) to enable near single photon detection in the deep UV. Digital control of integration allows the beginning and ending integration of detector output to correspond to any period before, during or after a deep UV excitation pulse. Each controller has a 32 MIP microprocessor with on-board 2M RAM and 256K flash memory to store detector calibration information including an individual gain/voltage lookup table to enable precise conversion of digital counts to incoming photons. Each DDC has on-board, on-the-fly, calibration of capacitor values and other components to ensure compensation of output readings for ambient temperature and other environmental factors.

Figure 8. Seven-channel digital detector controller

Another type of plug-and-play component designed to integrate and synchronize with our deep UV lasers is the miniature UV Raman monochromator shown below in Fig. 9. This monochromator employs an angle tuning filter with a 0.3 nm FWHM bandwidth, allowing Raman detection with a resolution about 40 cm^{-1} for detection of single Raman marker bands or about 15 cm^{-1} in a scanning mode with step size about 5 cm^{-1} to allow deconvolution of the Raman filter transmission spectra to allow higher Raman spectral resolution. This monochromator employs a single channel PMT controller shown integrated with a side looking Hamamatsu PMT module as well as a stepper motor with a 12 bit angular encoder, allowing angular resolution of the angle tuning filter to about 5 cm^{-1} spectral resolution. Software and graphical interface couple the deep UV laser, Raman band spectral location, and gated PMT detection and digitization to enable optimum signal to noise extraction of Raman information.

Figure 9. Miniature deep UV Raman monochromator

These and many more plug-and-play components were developed to allow easy integration of complete targeted ultraviolet chemical sensors.

3.3 Standard targeted UV chemical sensors

Two versions of the standard TUCS1000 are for surface and water contamination sensing. The surface sensor version is shown below in Fig. 10 and the water version shown in Fig. 11. The surface sensor version of TUCS1000 has been tested in Antarctica and the Arctic on several missions. The TUCS1000 is configured with 6 channels of detection including a combination of Raman and native fluorescence, plus a detector to measure outgoing laser energy or number of photons in an outgoing laser pulse. As described above, the sensor system has on-board calibration of all detector components including laser, integration capacitors, etc., so that accurate measurements are made of the number of photons collected in each detection band, whether Raman or native fluorescence. In typical use the sensor operates at spectral accumulation rates up to about 5 Hz and collects ambient background (without laser firing) for each spectral data set to allow ambient subtraction. Spectral accumulation rates up to 20 Hz are possible. The onboard microprocessor has a lookup table for the gain/voltage of each PMT and on-the-fly calibration of electronic component values to allow accurate backward calculation of the number of incident photons collected in each spectral channel, independent of PMT gain or voltage or automatically selected PMT output integration capacitance, adjusted to optimize signal to noise for each detection channel. Most of the detection of biological and organic detection is performed in UV spectral band where, together with the gated detection, eliminate ambient background due to sunlight. The sensor is therefore essentially solar blind. The present water TUCS is configured for detection and identification of contaminants in a water sample contained in a cuvette. The sensitivity of the water TUCS is 1 bacterial spore within the 0.1 mL active volume of the laser beam or 10 bacterial spores per mL with a signal to noise ratio of 100:1 (4000 counts with 40 counts of noise). The instrument can be configured to measure down to about 3 bacterial spores per liter. The instrument can be also be configured as a sipper system for continuous monitoring with a flow cell and pump, or for remote sensing of water contaminants similar to the surface version. BSA, a Ricin analog, was measured down to 2nM (50 ppb) and Trp down to less than 5 nM (1 ppb).

Figure 10. Surface version of TUCS1000

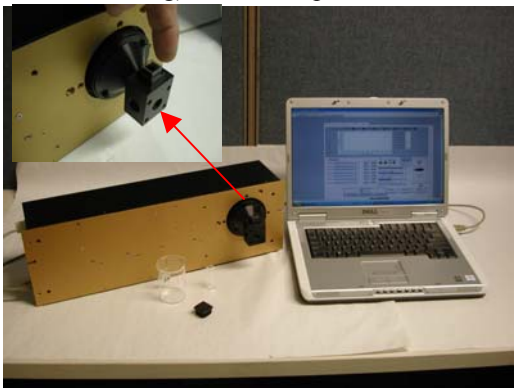

Figure 11. Water version of TUCS1000

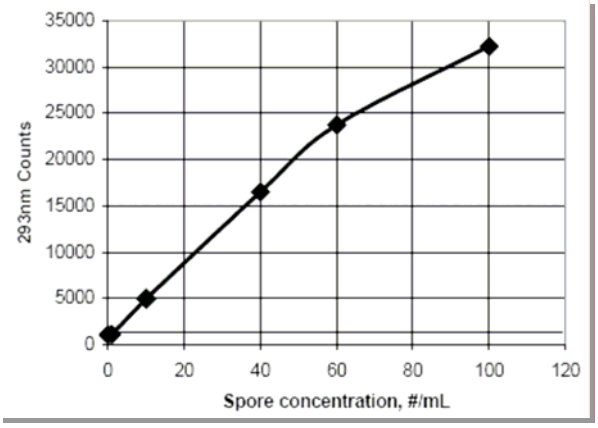

Figure 12. Digital detection counts in a 293 nm, 30 nm wide, detection band for B. subtilis bacterial spores in water

Both the surface and water versions of the TUCS1000 sensor have been operated on a standard camera battery for over 8 hours without recharging.

3.4 Examples of custom targeted UV chemical sensors

Below are photo's of a few examples of custom TUCS instruments including an instrument, the insides of which are shown on the left of Fig. 13, of a 5" diameter, 28" long instrument that was employed on several deep dives in the Pacific Ocean down to a depth about 8600 feet to detect and identify bacteria living in an around deep ocean vents. A second instrument is shown on the right of Fig. 13 of a small bore ice probe with an outside diameter of 2" which was deployed in ice holes in Antarctica in early 2006. This probe was designed for side viewing of bacterial populations within an ice column.

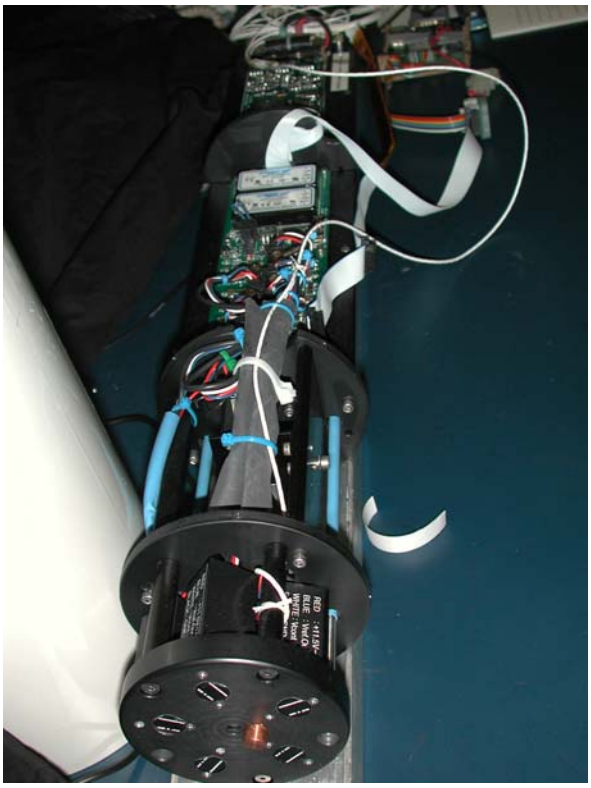

Figure 13. Photos of custom TUCS instruments for deep Ocean and deep ice Antarctic missions

4. SOFTWARE AND GRAPHICAL INTERFACE

Control and real-time data analysis of the targeted UV chemical sensors is performed through a LabView graphical interface that has an overall sensor control screen and separate component level control screens for: initial setup; laser control to setup laser energy, pulse width and pulse shape; PMT control to setup manual control of individual PMT gain, integration capacitor size and beginning and ending integration times, monochromator control to setup either angle tuning UV Raman monochromators or grating tuned scanning monochromators and select the output format for wavelength, frequency, or Raman shift. Raw PMT digital counts as well as normalized detected photon counts are displayed as well as ratios of incoming to outgoing laser photons. The basic sensor control screen is shown in Fig. 14 where the PMT setup screen is displayed with tabs along the top of the display for selection of other component level control screens.

Shown in Fig. 15 is the Main Page for operating a TUCS instrument. Via this screen acquisition of spectral data is accomplished with a single button where the TUCS instrument automatically maximizes signal to noise ratios, takes a set of spectral data, allows the user a decision to save or "learn" the spectral data into a data set, displays the normalized spectrum collected, and compares the data set against a library of "learned" data using principal component analysis (PCA). The new data set is displayed along with other "learned" data as a 2D PCA display showing the location of the new data compared to "learned" data in memory. The scalar distance in PCA space between the new data set and all other data sets or selected data sets in memory are displayed as a "Relatedness Index" from which a list of most likely matches is displayed in order to closeness. Also, displayed is the ratio of detected photons compared to outgoing photons to give an indication of the strength of the detected signal. On the left of Fig. 15 is a list of "learned" data sets so that a new spectral data set can be compared in PCA space against all or selected data sets in memory.

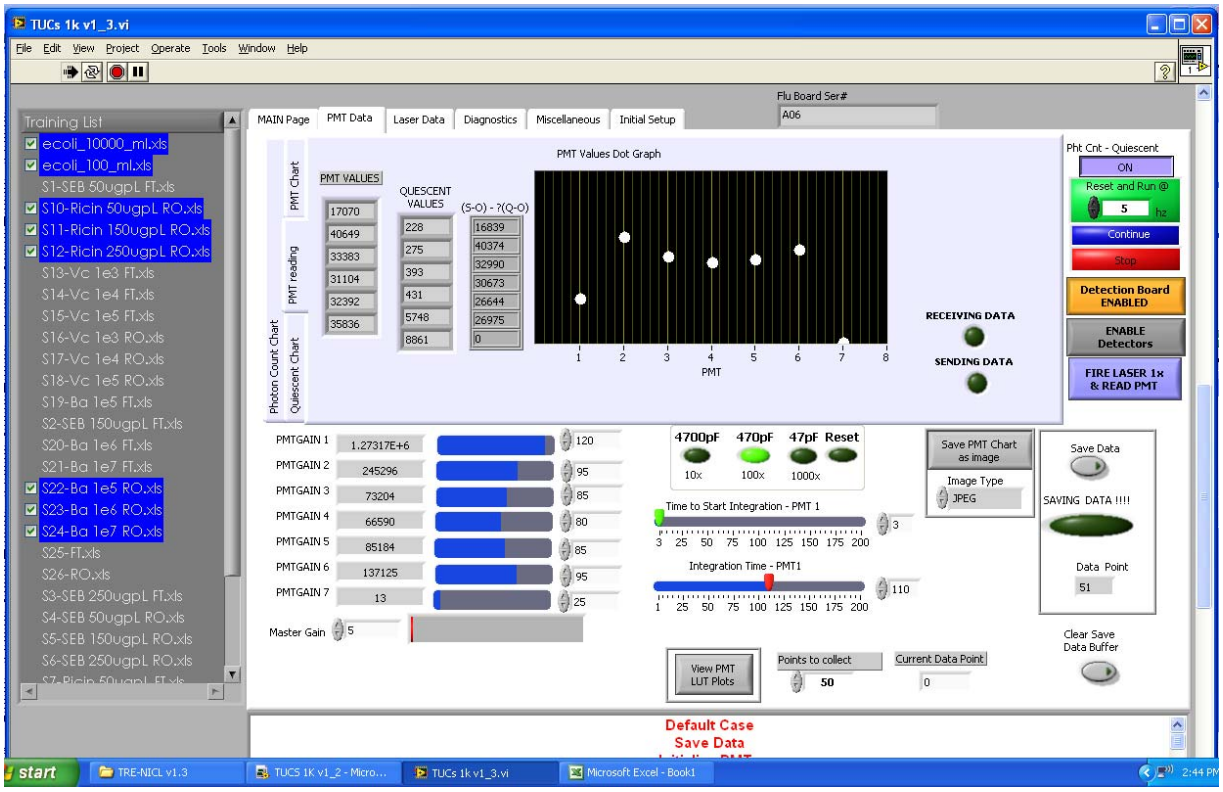

Figure 14. Typical control screen for PMT setup for a targeted UV chemical sensor

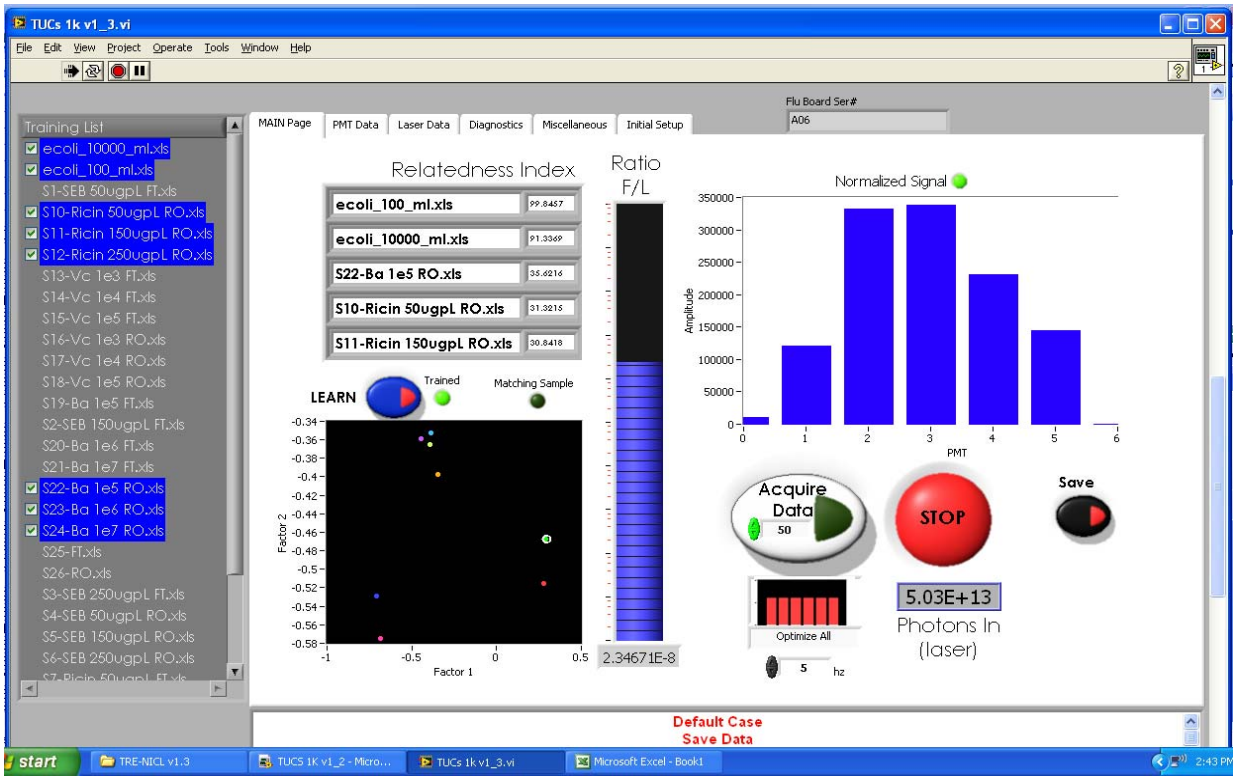

Figure 15. Main Page TUCS control screen

Figure 16, below, is an example of identification by sequential PCA[12]. In the 2D PCA graph on the left side of Fig. 16, the relative PCA location is displayed of 6 different samples of crude oil samples from different areas. Four of the crude oil sample are known and stored in the data base in the TUCS instrument. The identity of the two other samples is determined first by a stepwise process: first it is noted that the unknowns are not close to two of the four knowns. This allows the two non-proximate knowns to be de-selected from the PCA comparison base so that an amplified view of the PCA comparison can be made of the two remaining knowns and two unknowns, shown in the right portion of Fig. 16.

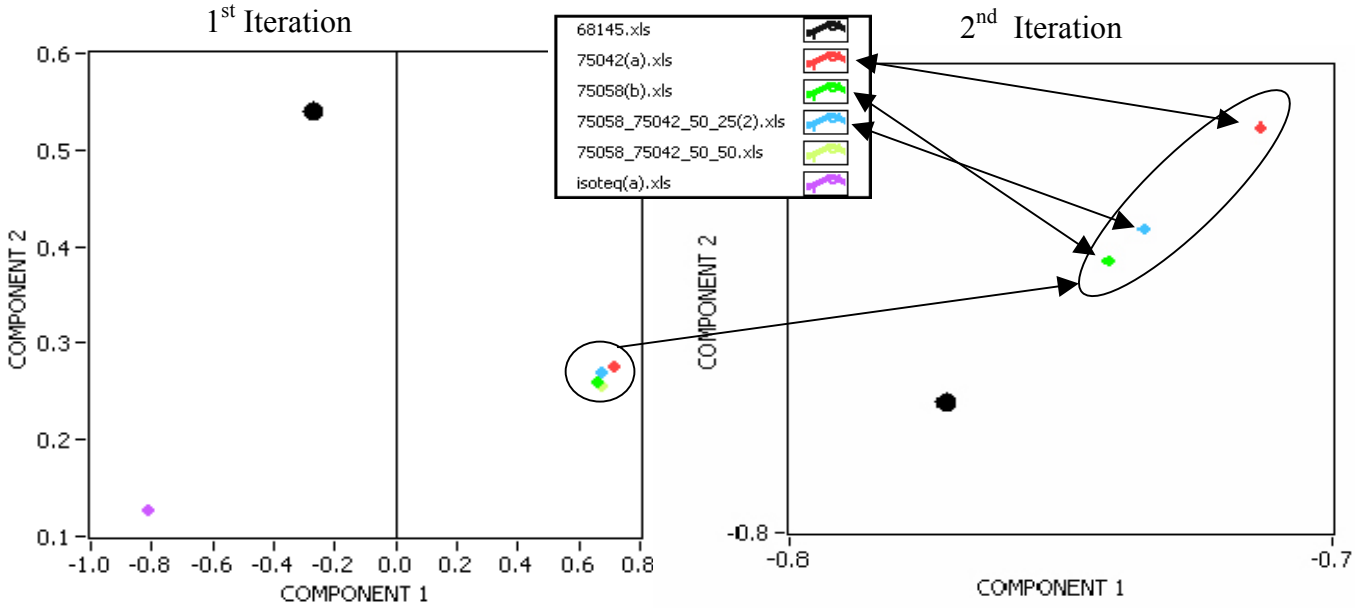

Figure 16. Chemical identification by sequential PCA iteration.

This comparison is so selective that sebum (skin oil) from four employees was tested and allowed identification of the individual to whom the samples belonged.

The TUCS operating software is ideal for use in relatively closed environments where the list of target and background materials is limited. In municipal or industrial wastewater the major offending target materials as well as background materials are fairly well described. This is also often the case in detecting and identifying contaminants in clean rooms, in manufactured food or chemical products, or testing air or water on the International Space Station. In each of these environments, the TUCS instrument can "learn" the environment and adapt to it, making more accurate contaminant identification along the way.

5. EXTENSIONS OF METHODS TO CAPILLARY ELECTROPHORESIS AND HIGH PERFORMANCE LIQUID CHROMATOGRAPHY

Capillary electrophoresis and high performance liquid chromatography are two methods of separating analytes in liquid buffers that enable accurate identification of chemical constituents. The identity of a chemical compound is determined by the separation time from the beginning of a separation until an unknown band peaks at the location of the detector. A major problem with both methods is that in order to make positive chemical identification it is necessary to normalize out variations in separation time. This is accomplished by running separations using known compounds as standards, immediately before and/or after a separation has been conducted. This ensures that variations in separation time due to ambient temperature and other variants are accounted for. An alternative method is to use a modest amount of spectral information to identify the differences in analyte constituents, thereby eliminating the need for running standards, which often take more than one hour in addition to the actual separation. The spectral methods are the same as described in this paper. Photon Systems' deep UV lasers and digital detector controllers and LabView software similar to that described above were employed in a recently published paper[13]. In this paper it is concluded that limits of detection for

dopamine, serotonin, and other neurotransmitters at the subcellular level of concentration were differentiable with limits of detection below 40 nM or 40 n mole L^{-1}. Similar techniques have demonstrated detection of unique compounds in high performance liquid chromatography down to the 5 nM range for proteins such as ibuprofen. This is a factor over 100,000 lower LODs than for commercial absorption detectors and over 1000 lower LODs than for commercial spectrofluorimeters. Demonstrated LODs are similar or lower than obtained with deep UV lasers that are over 500X larger, use over 3000X more power, and are up to 50X more expensive.

6. CONCLUSIONS

Hand-held, battery powered, reagentless, biological and chemical agent sensors are emerging that employ a combination of UV resonance and pre-resonance Raman and native fluorescence spectroscopy with the demonstrated ability to detect trace levels of biological and chemical contaminants, down to the level of a single spore at working distances of several meters. Rugged and reliable sensors have already been developed and demonstrated in very harsh conditions from the Artic to the Antarctic to the deep Ocean. Software has also been demonstrated with the ability to distinguish minute differences in chemical compositions of similar materials.

These techniques have also been extended to detectors for capillary electrophoresis and high performance liquid chromatography, where limits of detection down to a few nanomolar corresponding to attomole to zeptomole amounts of material have been demonstrated and multi-spectral techniques have been shown to be able to eliminate the need for running lengthy standards tests to establish separation times for both CE and HPLC.

7. ACKNOWLEDGEMENTS

We would like to thank NASA and Jet Propulsion Laboratory for their support of this work.

REFERENCES

[1] Relman, D.A., "Detection and Identification of Previously Unrecognized Microbial Pathogens", Emerging Infectious Diseases, Vol.4, No. 3, July-Sept. 1998.
[2] S.A.Asher, C.R. Johnson, "Raman Spectroscopy of a Coal Liquid Shows That Fluorescence Interference Is Minimized with Ultraviolet Excitation", Science, 225, 311-313, 20 July 1984.
[3] Asher, S.A. and C.R. Johnson, "UV Resonance Raman Excitation Profile Through the $^1B_2$ State of Benzene", J. Phys. Chem. Vol89, 1985, pp. 1375-1379.
[4] Li, B., and A.B. Myers, "Absolute Raman Cross Sections for Cyclohexane, Acetonitrile, and Water in the Far Ultraviolet", J. Phys. Chem. Vol94, 1990, pp. 4051-4054.
[5] Christesen, S., J.M. Lochner, A.M. Hyre, and Darren K. Emge, "UV Raman Spectra and Cross Sections of Chemical Agents", SPIE, Vol. 6218, 621809, April, 2006.
[6] Sparrow, M.C., J.F. Jackovitz, C.H. Munro, W.F. Hug, and S.A. Asher, "A New 224nm Hollow Cathode UV Laser Raman Spectrometer", App. Spect., Vol. 55, No. 1, Jan 2001.
[7] Asher, S.A., "UV Raman Spectroscopy", Anal. Chem., Vol. 65, 1993, p. 59 and 210.
[8] Nelson, W.H., R. Manoharan and J.F. Sperry, "UV Resonance Raman Studies of Bacteria", App. Spect. Reviews, 27 (1), pp. 67-124, 1992
[9] Wu, M., M.Ray, K.H.Fung, M.W. Ruckman, D. Harder, and A.J. Sedlacek, "Stand-off Detection of Chemicals by UV Raman Spectroscopy", App. Spect., Vol.54, No.6, 2000, pp. 800-806.
[10] W.H.Hug, R.Bhartia, A.Tsapin, A.L.Lane, P.G.Conrad, K. Sigapati, and R.D. Reid, "Status of Miniature Integrated UV Resonance Fluorescence and Raman Sensors for Detection and Identification of Biochemical Warfare Agents", Proc. SPIE, Vol. 5994, p5884J1-12, Boston, MA. Oct. 2005.
[11] R.Bhartia, W.F.Hug, E.C.Salas, K.Sijapati, A.L.Lane, R.D.Reid and P.G.Conrad, "Biochemical detection and indentification false alarm rate: dependence on wavelength using laser induced native fluorescence", Proc. SPIE, Vol.6218, Orlando, FL. Apr. 2006.
[12] Bergan, T and M.P. Starr " Sequential principal components analysis, a tool for cluster detection in large bacteriophage-typing data samples" Current Microbiology 6:1 1981 p1-6.
[13] T.Lepainis, C. Scanlan, S.S.Rubakhin, and J.V. Sweedler, "A multichannel native fluorescence detection system for capillary electrophoretic analysis of neurotransmitters in single neurons", J. Anal.Bioanal. Chem., Hhttp://dx.doi.org/10.1007/s00216-006-0775-9H, 1618-2642 (Print), Springer-Berlin, Sept. 20, 2006.